

# Mutually orthogonal Golay complementary sequences in the simultaneous synthetic aperture method for medical ultrasound diagnostics. An experimental study

Y. Tasinkevych<sup>\*</sup>, I. Trots, A. Nowicki

*Ultrasound Department, Institute of Fundamental Technological Researches Polish Academy of Sciences, Poland*



## ARTICLE INFO

### Keywords:

Coded excitation  
Mutually orthogonal Golay codes  
Synthetic aperture  
Ultrasound imaging

## ABSTRACT

Complementary Golay coded sequences (CGCS) have several advantages over conventional short pulse transmitted signals. Specifically, CGCS allow the signal-to-noise ratio (SNR) to be increased. Moreover, due to matched filtering and compression, echoes resembling the short pulse waveform with substantially higher amplitude can be obtained. However, CGCS require two subsequent transmissions to obtain a single compressed signal. This decreases the data acquisition rate and the frame rate of ultrasound imaging by two-fold. To alleviate this problem, mutually orthogonal Golay complementary sequences (MOGCS) can be used. MOGCS allow the simultaneous transmission of two CGCS pairs to be implemented, yielding the acoustic data for two image frames in one data acquisition cycle.

The main objective of this work was an experimental study of the most crucial parameters of the received acoustic signals, e.g. the signal-to-noise ratio (SNR), the side-lobes level (SLL) of the signal and the axial resolution, obtained from simultaneous transmission of two pairs of CGCS comprising a MOGCS set to demonstrate their feasibility of being used in ultrasonography. For this purpose, a simultaneous synthetic transmit aperture method (SSTA) was proposed. The SSTA is based on MOGCS transmission and simultaneous reconstruction of two image frames from a single data acquisition cycle. This doubles the image reconstruction rate in comparison with conventional CGCS signals.

In this paper, the ultrasound data from a perfect reflector, commercial phantoms and *in vivo* measurements were analysed. Two 16-bit long CGCS pairs comprising the MOGCS set were programmed and transmitted using the Verasonics Vantage™ research ultrasound system equipped with a Philips ATL L7-4 linear array ultrasound probe. It was shown that the signal parameters and overall quality of reconstructed B-mode images did not deteriorate when using the MOGCS in comparison to the conventional CGCS and short pulse signals explored so far.

## 1. Introduction

In ultrasound diagnostic image requirements are becoming more and more demanding. Penetration depth, signal-to-noise ratio (SNR), axial and lateral resolution, side-lobe level (SLL) and contrast-to-noise ratio are the most frequently used parameters characterising the quality of ultrasound images. The SNR and penetration depth depend on the energy dissipation along the propagation path due to acoustic wave attenuation in the surrounding medium. On the other hand, the axial and lateral resolutions of the ultrasound image depend on the frequency of the transmitted signal and the aperture size [1]. Attenuation of

ultrasound waves in tissue increases approximately linearly as a function of frequency [2] and limits the resolution at greater depths. Hence, the maximum penetration depth (dependent on SNR) and axial resolution (dependent on operating frequency) are the two most important and contradicting parameters in ultrasound imaging. Therefore, to visualise the deeper parts of the examined body, the peak power of the interrogating pulse must be increased. However, the maximum peak power is restricted by medical standards (IEC standard 60601-2-37). To overcome this difficulty, wide-band interrogating signals, and coded sequences in particular, can be applied [3]. The energy of the transmitted signal is proportional to the code duration. Compression, involving

\* Corresponding author.

E-mail address: [yurijtas@ippt.pan.pl](mailto:yurijtas@ippt.pan.pl) (Y. Tasinkevych).

match-filtering, allows for increasing the amplitude and the SNR of the recorded echoes and the penetration depth, without amplifying the transmitted signal [4]. This also allows the transmit frequency to be increased, which yields resolution improvement. Different approaches to the problem of signal compression and SNR improvement have been reported in the literature. For example, in [5] a ‘pseudo-chirp’ (*chirp* - linear frequency modulated signals) excitation and equalisation filtering was proposed for phased arrays imagers to increase the SNR of ultrasound images. In [6], a method based on pulse elongation and deconvolution, implemented as a stabilised inverse filter, was proposed to reduce the range side-lobes. The optimal waveform was obtained using a minimum mean-square error optimisation approach. In [7], the spectrally matched signals with constant amplitude and nonlinear frequency modulation were analysed for side-lobe reduction of the compressed pulses and in [8] pre-distorted chirp signals were studied experimentally to evaluate the influence of the frequency weighting from the transducer’s bandwidth on the efficiency of side-lobe reduction. Application of the Barker codes and mismatched filter for high-frequency ophthalmologic imaging was proposed in [9], whereas in [10] the pseudo-random binary sequence (*m*-sequence) was studied. Increased range resolution and SNR improvement over a short pulse signal were demonstrated experimentally through imaging evaluation and flow measurements. Recently, the Golay codes have been receiving growing attention in comparison to the other transmitted signals introduced by M. J. E. Golay in [11], these are also known as the complementary Golay coded sequences (CGCS). The CGCS have a unique property of total side-lobe suppression as a result of matched filtering and signal compression. The compressed waveform is similar to the conventional short pulse with much higher amplitude (theoretically, the amplitude increase can be up to  $2L$ , where  $L$  is the number of bits of the code sequence [12]). Fundamental properties of the CGCS, including matched filtering and compression techniques, were discussed in detail in [13]. The major drawback of the CGCS is that transmission of each sequence of the complementary pair has to be transmitted subsequently. This causes a two-fold reduction of the data acquisition rate which, in turns, results in a corresponding decrease in the ultrasound image reconstruction frame rate. The frame rate or the speed of image reconstruction is defined as the number of reconstructed images (frames) per second (fps) and is one of the most crucial factors in ultrasound medical imaging diagnostics. Apart from computational speed related to the image reconstruction algorithm implementation and the hardware used, it is physically limited by the speed of data acquisition, which depends on the acoustic wave speed in the medium, depth of visualisation and the number of scan-lines reconstructed. The main drawback of the CGCS, as mentioned above, can be alleviated by applying the mutually orthogonal Golay complementary sequence (MOGCS) excitation signals [14]. Mutual orthogonality (defined in the next section) allows for two different CGCS pairs (comprising a MOGCS set) to be transmitted simultaneously. The echoes corresponding to different complementary pairs can be extracted from the received signal and processed using CGCS matched filtering and compression techniques [13]. This enables simultaneous acquisition of the acoustic data for two image frames, thus compensating for the frame rate reduction due to the subsequent transmission of two CGCS.

Several ultrasound imaging approaches based on MOGCS transmitting have been reported in the literature [15–18]. In [15], the classical beamforming method based on ‘delay-and-sum’ dynamic receiver focusing B-mode imaging was proposed. A 64-element transducer array was divided into two parts comprised of even and odd numbered elements. Each part was excited with different 16-bit long pairs of a MOGCS set. Therefore, different CGCS pairs transmitted along different scanlines yielded two interlaced image frames. This method, however, required at least four consecutive transmissions to be combined in order to alleviate the grating lobe issue, which inevitably appeared due to every other element excitation. In [16], a simultaneous transmit multi-zone focusing method using modified orthogonal Golay codes designed for small-scale systems (e.g. hand-held, portable ultrasound systems) was discussed.

The sum of two MOGCS focused at two different depths was simultaneously transmitted along the same scan-lines and received with each array element. In this method, matched filtering was performed after beam-forming to simplify the system design, which introduced additional errors in the image reconstruction. The B-mode images of numerically simulated data were presented and no experimental verification was performed. Moreover, in this method, five states, i.e.  $\pm 2$ ,  $\pm 1$  and 0, of the transducer excitation voltage would be necessary. This would require complicated electronics especially when the number of transducer elements to be excited is large (192 elements in the cited work) and is inconsistent with the simplicity of small-scale systems design. In [17], a method for high frame rate sector imaging was proposed. It was based on simultaneous excitation of the MOGCS pair, each of them corresponding to the emission of a plane wave with a different transmission angle. The received echo signals corresponding to different angles were extracted and two images of different regions within the imaging area were obtained. Finally, the two images were combined into a single frame of the sector mode image. Similarly, as in [16], the sum of two MOGCS was transmitted simultaneously by every element, yielding similar system hardware design requirements as mentioned above. In [18], the approach analogous to [17] was used for the transmission of two diverging waves instead of plane waves to obtain a single frame of an even wider sector mode image. The majority of papers dealing with MOGCS excitation signals mainly concern the implementation of the classical beamforming (dynamic receive focusing) and plane or diverging wave imaging methods. The synthetic transmit aperture (STA) method, in contrast to the methods mentioned, provides full dynamic focusing in transmit and receive modes [19–21]. This allows high-resolution imaging to be obtained. In the STA method, several elements (up to 16 elemental transducers [21]) are used in transmit mode at any time. This limits the energy of the transmitted pulse-wave and visualisation depths. In this context, application of the CGCS and MOGCS in particular seems to be promising to alleviate this problem. Specifically, it was shown in [22], application of the  $L$ -bit long CGCS allowed for improving the SNR by approximately  $\sqrt{L}$  in comparison with the short pulse excitation signal in the case of B-mode images obtained using the STA approach. Some preliminary results of the MOGCS-based STA imaging are discussed in [23,24]. However, the analysis was limited to numerical simulations only and no experimental verification was conducted. In [23], the authors limited themselves to considering two-bit long MOGCS comprised of four pairs, thus repeating transmission of the same coded sequences several times (Eq. (5) in [23]), which is misleading. Moreover, the mutual orthogonality property for the elements of a MOGCS set comprised of four CGCS (Eq. (4) in [23]) was incorrectly defined. Specifically, according to [14], the sum of all cross-correlations must vanish; therefore, the expression for partial echoes extraction from the received signal (Eq. (6) in [23]) leads to incorrect results. In turn, in [24], the possibility of MOGCS application in STA is briefly mentioned only in the context of classical beam-forming and plane-wave imaging methods discussed in the cited works [15–17]. The work presents preliminary results of numerical simulations without profound comparative analysis and experimental verification. Furthermore, no profound analysis of the MOGCS radio-frequency (RF) echoes showing the efficiency of match filtering (i.e. extraction of the echoes corresponding to different CGCS pairs comprising the MOGCS set from the received signal) in the case of experimentally obtained data has been reported in the literature so far.

The main objective of this work is the experimental study of the RF signals obtained as a result of the simultaneous transmission of two CGCS pairs comprising a MOGCS set to demonstrate their feasibility for use in ultrasound diagnostics. For this purpose, the acoustic echoes from a brass plate modelling a perfect reflector and from a general purpose phantom (model 525, Dansk Fantom Service [25]) were measured, analysed and compared for different excitation signals. Specifically, such parameters of the received signals, like the pulse duration at the –6

dB and  $-20$  dB levels, the signal SLL and the SNR, obtained from simultaneous transmission of two 16-bit long CGCS pairs comprising a MOGCS set were estimated and compared with those obtained using conventional CGCS and short (one-sine cycle of operating frequency) pulse signals. For MOGCS and CGCS transmissions, the received signals were first processed with matched filters in order to extract corresponding echoes (MOGCS) and compress them to suppress the signal side-lobes. Next, the signal parameters were determined and compared to those of the short pulse transmitted signal. Experimental measurements were conducted using a Verasonics Vantage<sup>TM</sup> commercial ultrasound system (Verasonics Inc., Kirkland, WA, USA) equipped with a Philips ATL L7-4 linear array ultrasound probe.

Moreover, the simultaneous synthetic transmit aperture (SSTA) imaging method based on the simultaneous transmission of two CGCS pairs comprising a MOGCS set and simultaneous reconstruction of two image frames was proposed and studied using experimental data. The method illustrates the simultaneous reconstruction of two high-resolution B-mode image frames obtained using MOGCS acoustic echoes from a single data acquisition cycle and presents a comparison with B-mode images obtained using conventional short pulse and CGCS transmitted signal. For this purpose, the STA acoustic data were collected from a general purpose phantom (model 525, Dansk Fantom Service [25]) and a cyst phantom (model 571, Dansk Fantom Service [26]). Moreover, the STA data were acquired *in vivo* by imaging the abdominal aorta and common carotid artery of a human volunteer (one of the co-authors). The B-mode images were synthesised and compared for the proposed SSTA with MOGCS signals and conventional STA with short pulse and CGCS excitation signals. To the authors' best knowledge, experimental studies of STA imaging with simultaneous frame synthesis using MOGCS signals has not been explored in the literature so far.

The rest of the paper is organised as follows. The next section presents a brief overview of the theoretical aspects of the CGCS and MOGCS. In the Section 3, the details of the experimental set-up are explained. Sections 4 and 5 present the experimental results obtained using MOGCS, CGCS and short pulse transmitted signals and the discussion, respectively. Finally, Section 6 briefly summarises the presented work.

## 2. Theory

The main advantages of the CGCS over the short pulse transmitted signal are the ability to obtain a compressed signal with suppressed side-lobes and SNR improvement. However, in contrast to the short pulse, the CGCS requires two consecutive transmissions to obtain the compressed signal. This means that data acquisition takes two times longer for the CGCS in comparison to the short pulse. This drawback can be successfully overcome by applying the MOGCS signal [14]. Concretely, consider two  $L$ -bits long CGCS pairs  $A_i$  and  $B_i$ ,  $i = 1, 2$ , (i.e.,  $A_1 A_2$  is a complementary pair #1 and  $B_1 B_2$  is a complementary pair #2) which obey the following condition [13]:

$$R_{A_1}(n) + R_{A_2}(n) = \begin{cases} 2L, & n = 0 \\ 0, & n \neq 0 \end{cases}, \quad R_{B_1}(n) + R_{B_2}(n) = \begin{cases} 2L, & n = 0 \\ 0, & n \neq 0 \end{cases} \quad (1)$$

The autocorrelation function of the coded sequence in Eq. (1) is defined as follows [28]:

$$R(n) = \begin{cases} \sum_{k=0}^{L-1-n} S(k)S(k-n), & n = 0 \dots L-1, \\ R(-n), & n = -(L-1) \dots -1, \end{cases} \quad (2)$$

where  $S(k)$ ,  $k = 0 \dots L-1$  denotes the coded sequence  $A_i$ ,  $B_i$ ,  $i = 1, 2$  of the length  $L$ . Furthermore, the two CGCS pairs  $A_i$  and  $B_i$  are said to be mutually orthogonal pairs, or MOGCS pairs, if the sum of the corresponding cross-correlation functions vanishes

$$\sum_{i,j=1}^2 R_{A_i B_j} = 0. \quad (3)$$

The cross-correlation functions in Eq. (3) are defined as follows [27]:

$$R_{A_i B_j}(n) = \begin{cases} \sum_{k=0}^{L-1-n} A_i(k)B_j(k-n), & n = 0 \dots L-1, \\ \sum_{k=0}^{L-1-n} A_i(k-n)B_j(k), & n = -(L-1) \dots -1, \end{cases} \quad (4)$$

Thereby, the CGCS pairs  $A_i$  and  $B_i$ ,  $i = 1, 2$ , comprise the MOGCS set if they simultaneously obey Eqs. (1) and (3). The main consequence of the mutual orthogonality, defined in Eq. (3), is the ability to transmit two CGCS pairs simultaneously. The echoes corresponding to different CGCS pairs comprising the MOGCS set can be efficiently extracted from the received signal using the Golay codes compression algorithm, briefly discussed below. Specifically, consider an example of the MOGCS set comprised of two 16-bit long CGCS pairs  $\{A, B\}$  shown in Table 1 (similar codes were used in the experimental measurements):

The sequences  $\{A_i, B_i\}$  are transmitted by two adjacent elements {say, #1 and #2} of the array transducer. Specifically, the Golay coded sequences  $\{A_1, B_1\}$  are transmitted first. Then the corresponding echoes are detected and stored in the memory for further processing. Next, the procedure is repeated for the sequences  $\{A_2, B_2\}$ . The partial echoes corresponding to the Golay coded sequences  $\{A_i, B_i\}$ ,  $i = 1, 2$  can be extracted from the received signals and compressed by adding together the cross-correlation functions of each of the received signals with corresponding transmitted sequences. Concretely, in order to recover the echo corresponding to the sequence  $A = \{A_1, A_2\}$  transmitted by the transducer element #1, for the first and the second transmissions, one should compute the sum of cross-correlation functions of the received signals  $S_i$  with corresponding transmitted codes  $A_i$ ,  $i = 1, 2$  using Eq. (3) as follows:

$$P_A = \sum_{i=1}^2 R_{S_i A_i} \quad (5)$$

In this work, the cross-correlation functions were computed in Matlab® using *xcorr* routine from the *Signal Processing Toolbox*.

It should be noted that Eqs. (1) and (3) can be generalised on  $M$  MOGCS sets, each comprised of  $M/2$  CGCS pairs [14]. In this case, however, the mutual orthogonality property of any two MOGCS sets means that the sum of all combinations of the cross-correlation functions computed for all  $M/2$  CGCS pairs in each of the two MOGCS sets must vanish. Extraction of the particular echoes from the received signal resulting from simulations transmission of  $M$  CGCS pairs is not as obvious and straightforward anymore.

## 3. Method

A pair of 16-bit long CGCS, two pairs of 16-bit long CGCS comprising a MOGCS set and a short pulse (one sine-cycle) at a nominal frequency of 5.2 MHz and 20.83 MHZ sampling rate were generated by the Verasonics Vantage<sup>TM</sup> (Verasonics inc., Kirkland, WA) research ultrasound system equipped with the Philips ATL L7-4, 128 elements linear array transducer. The block diagram of the experimental setup is shown in Fig. 1.

First, the ultrasound echoes from a perfect reflector (brass plate immersed in a tank filled with degassed water) were collected. The signals obtained from the reflector allowed the efficiency of MOGCS and CGCS compression to be assessed. For this purpose, the compressed signal duration at  $-6$  dB and  $-20$  dB amplitude levels were measured

**Table 1**  
16-bit long CGCS comprising a MOGCS set.

$A_1$	1 1 1 -1 1 1 -1 1 1 1 1 -1 -1	$A_2$	1 1 1 -1 1 1 -1 1 -1 -1 1 1 1 -1
	-1 1 -1		1
$B_1$	1 -1 1 1 1 -1 -1 -1 1 -1 1 1 -1	$B_2$	1 -1 1 1 1 -1 -1 -1 1 -1 1 1 -1
	1 1 1		-1 -1

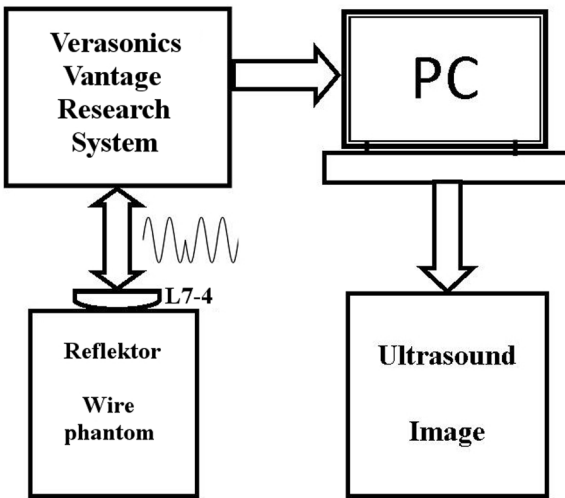


Fig. 1. Block diagram of the experimental setup.

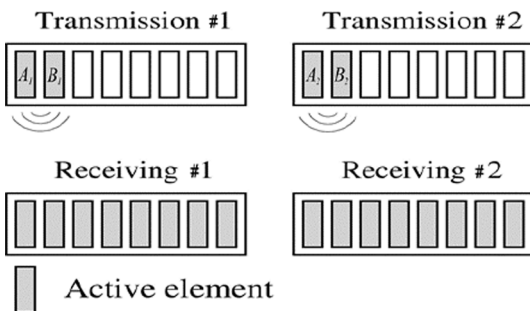


Fig. 2. STA acoustic data acquisition diagram using two pairs of CGCS comprising the MOGCS excitation signal.

and compared to that of the short pulse. Also the SLL (defined here as the ratio of the side-lobes level to the main-lobe level of the signal envelope) was determined using the signals reflected from the brass plate and compared for the three modalities tested, i.e. MOGCS, CGCS and short pulse, respectively. To compare the SNR, the ultrasound RF echoes were collected from the general purpose phantom with attenuation 0.5 dB/[cm × MHz] (which corresponded to 5.7 Np/[m × MHz]). The SNR, defined here as the ratio of the average signal power to the RMS noise power [28] was determined at different depths from the recorded RF signals and from the echoes along the central line of the synthesised B-mode images of the general purpose phantom and compared for the MOGCS, CGCS and short pulse excitation signals. The average signal power was computed over the echo samples in the 1.5 mm (5 wavelengths, the wavelength approximately equals 0.3 mm) window centred around the peak amplitude at given depth, whereas the RMS noise power was computed over the samples in the 10 mm (about 34 wavelengths) window starting from 100 mm where practically no signal is observed and only noise is present (see Fig. 5 and Fig. 7). For computing the SNR, SLL and axial resolution the sample rate of corresponding signals was increased by a factor of 16 in Matlab® using the *interp* routine.

Finally, simultaneous reconstruction of two high-resolution image frames from acoustic data obtained using the MOGCS signal collected during a single data acquisition cycle was demonstrated. For this purpose, the STA data were collected from the general purpose phantom and the cyst phantom. Moreover, the STA data were also acquired *in vivo* using the human abdominal aorta and common carotid artery of a volunteer (one of the co-authors). Longitudinal scans of both arteries were performed using all three modalities tested, i.e. MOGCS, CGCS and

short pulse, respectively. The B-mode images obtained using the proposed SSTA image reconstruction method with the MOGCS excitation signals and the conventional STA method with the CGCS and short pulse excitation signals were compared.

### 3.1. Simultaneous synthetic transmit aperture imaging method

To gain insight into the SSTA image reconstruction method proposed here, it might be appropriate to consider the STA data acquisition scheme shown in Fig. 2. This diagram depicts the case in which two CGCS pairs  $A = \{A_1, A_2\}$  and  $B = \{B_1, B_2\}$ , comprising the MOGCS set (see Table 1) are transmitted by two adjacent elements of a linear array transducer. Specifically, the transducer array element #1 transmits the code  $A_1$  and the element #2 transmits the code  $B_1$  during the first transmission of the MOGCS. Next, the element #1 transmits the code  $A_2$  and the element #2 transmits the code  $B_2$  during the second transmission. In both transmit events the ultrasound echoes are acquired simultaneously by all elements of the transducer array in receive mode. Next, the transmit sub-aperture is moved along the transducer by a specified number of elements. In the experimental results shown in the next section, the two-element stride was applied. Therefore, for the example considered, elements #3 and #4 are used in the next acquisition in transmit mode and all elements are recording back-scattered signals. This process is repeated until the last element of the probe is reached.

When the data acquisition cycle is finished, the RF signals are processed using the SSTA image reconstruction method proposed here. Specifically, first the echoes corresponding to the CGCS  $A = \{A_1, A_2\}$  and  $B = \{B_1, B_2\}$  are extracted. To this end, the cross-correlations defined in Eq. (3) are computed for the codes  $A = \{A_1, A_2\}$  and  $B = \{B_1, B_2\}$  and all 128 RF signals recorded for each transmit sub-aperture. This yields 128-by-64 compressed echoes corresponding to the CGCS  $A = \{A_1, A_2\}$  and  $B = \{B_1, B_2\}$ . These echoes comprise two STA RF data sets corresponding to the transmitted CGCS  $A = \{A_1, A_2\}$  and  $B = \{B_1, B_2\}$ , respectively. Next, the RF data sets are processed using conventional STA image reconstruction method simultaneously, yielding two B-mode image frames - 'frame A' and 'frame B' (see notation of the examples shown in the next section).

The same two-element transmit sub-aperture and two-element stride were used for the short pulse excitation and conventional CGCS excitation signals. In the case of CGCS excitation signal, only one complementary pair  $A = \{A_1, A_2\}$  (see Table 1) was transmitted. The RF data were recorded and processed using the conventional STA method [21] and the obtained images were compared with those obtained using the SSTA image reconstruction method.

For the case of the MOGCS and CGCS excitations, a full data acquisition cycle required 128 transmissions and 16,384 RF signals were recorded. In the case of the short pulse only 64 transmissions and 8192 RF signals were required. The raw data were collected with the sampling rate of 20.83 MHz and stored in the PC memory for further processing. All signal processing algorithms mentioned above were implemented in Matlab®.

## 4. Results

### 4.1. Perfect reflector measurements

The RF signals detected from the perfect reflector for different transmitted signals are shown in Fig. 3.

Specifically, the short pulse echo is shown in Fig. 3(a). The RF echoes, being a superposition of the 16-bit long MOGCS codes  $A_1$  and  $B_1$ ,  $A_2$  and  $B_2$ , are shown in Fig. 3(b) and Fig. 3(c), respectively. Similarly, the echoes corresponding to the CGCS sequences  $A_1$  and  $A_2$  are shown in Fig. 3(d) and (e). The signals were transmitted by elements #63 and #64 and recorded by element #64 of the probe. All RFs collected were normalised to their maximum values.

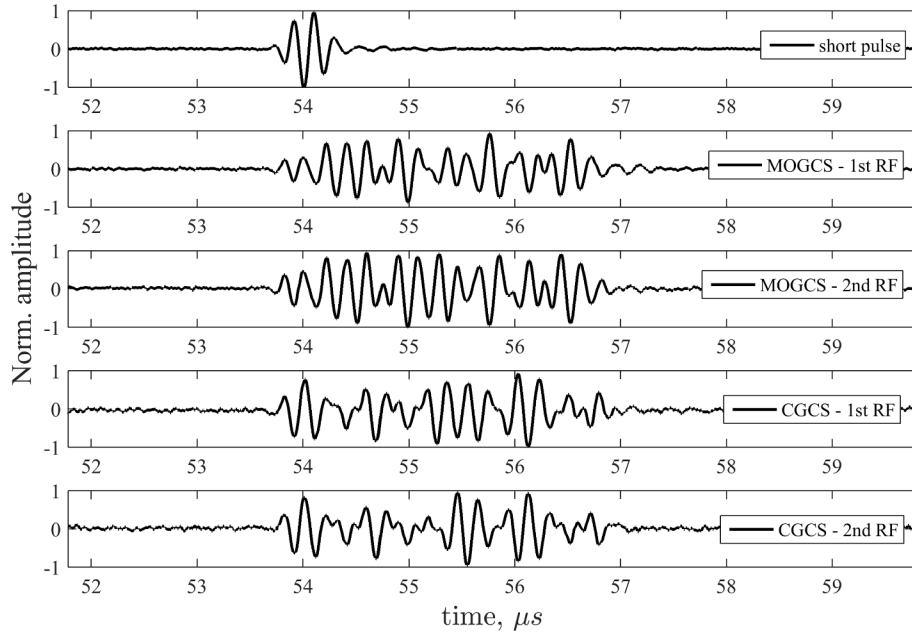


**Fig. 3.** Normalised RF signals collected from the perfect reflector for the short pulse transmission (a), the MOGCS echo being a superposition of the codes  $A_1$  and  $B_1$  (b), the MOGCS echo being a superposition of the codes  $A_2$  and  $B_2$  (c), the CGCS echo resulting from  $A_1$  sequence transmitted (d), the CGCS echo resulting from  $A_2$  sequence transmitted (e). Elements #63 and #64 were used in transmit mode; the echoes were detected by element #64.

In Fig. 4, the envelopes of the signals reflected from the brass plate (see Fig. 3) are shown. In the case of MOGCS and CGCS signals, the RF echoes were compressed using the match filtering technique prior to envelope detection. For the MOGCS, the envelope of code A is shown only. The same code  $A = \{A_1, A_2\}$  was used as the CGCS example in the Fig. 3(d) and (e). The half maximum (measured at the  $-6$  dB level) time duration of the envelopes for the MOGCS and CGCS was determined to be  $0.33 \mu s$  and  $0.3 \mu s$ , respectively. The corresponding value for the short pulse was  $0.36 \mu s$ . The above values of the time duration expressed in units of spatial distance were  $0.51 \text{ mm}$  and  $0.46 \text{ mm}$  for coded excitation

MOGCS and CGCS, respectively. The corresponding value for the short pulse excitation was  $0.55 \text{ mm}$ . The time duration of the envelopes measured at the  $0.1$  level ( $-20 \text{ dB}$ ) were  $0.58 \mu s$  for the MOGCS,  $0.6 \mu s$  for the CGCS and  $0.61 \mu s$  for the short pulse transmission. These corresponded to  $0.89 \text{ mm}$  for the MOGCS,  $1.01 \text{ mm}$  for the CGCS and  $0.94 \text{ mm}$  for the short pulse transmission, respectively.

In Fig. 4, the SLL values determined at specific points of the curves are also shown. Specifically, the SLL values for the MOGCS and CGCS signals were at least  $-20.6 \text{ dB}$  and  $-22.2 \text{ dB}$ , respectively. The corresponding value for the short pulse was  $-20.1 \text{ dB}$ .

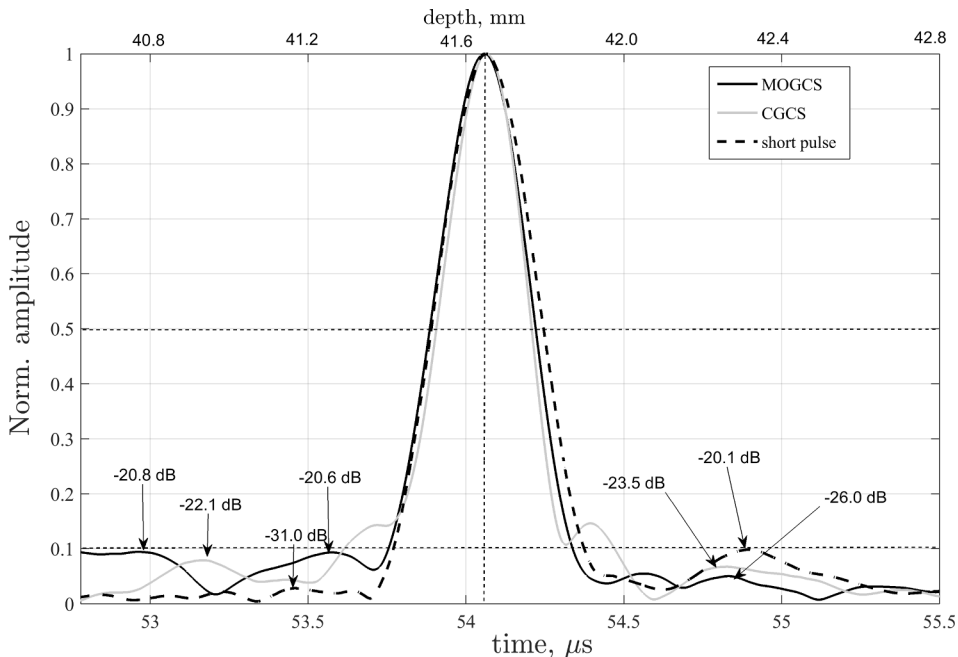


**Fig. 4.** The normalised envelopes of the processed RF echoes obtained from the perfect reflector using the short pulse, the MOGCS and the CGCS transmitted signals. Elements #63 and #64 were used in transmit mode; the echoes were detected by element #64. The text arrows show the SLL values determined at specific points of the curves.

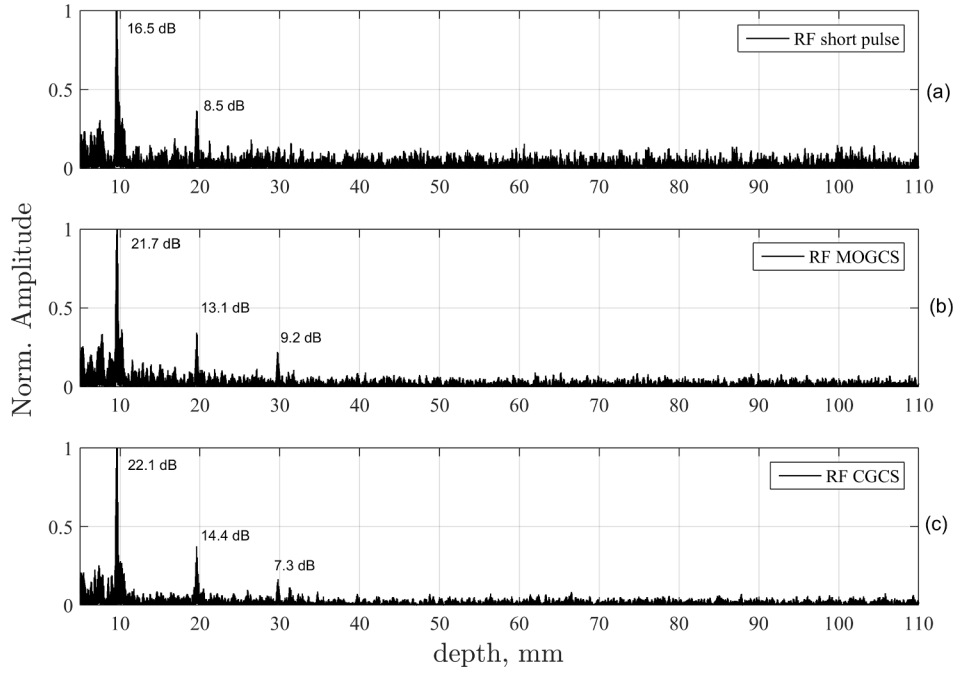


**Fig. 5.** The normalised amplitudes of the received RF echoes obtained from the general purpose phantom using the short pulse (a), the MOGCS (b) and the conventional CGCS (c) transmission. The absolute values of the received echoes are shown. Elements #63 and #64 were used in transmit mode; the echoes were detected by element #64. For the peaks of the echo amplitudes, the SNR values are shown.

#### 4.2. Phantom measurements

In Fig. 5, the normalised amplitudes of the received echoes collected from the general purpose phantom are shown.

The echoes were recorded using element #64 of the probe; the peak-to-peak transmitted voltage was set to a value of 3.2 V to emphasise the advantage of the MOGCS and CGCS over the short pulse excitation. The recorded echoes were normalised to their maximum values. The range of depth for which it was possible to determine the SNR for short pulse signal was limited to 20 mm. The SNR values estimated for the MOGCS signal at the depths of 10 mm, 20 mm and 30 mm were 21.7 dB, 13.1 dB and 9.2 dB and 22.1 dB, 14.4 dB and 7.3 dB for the conventional CGCS

signal. In the case of the short pulse, the corresponding values at the depths of 10 mm and 20 mm were 16.5 dB and 8.5 dB, respectively.

The B-mode images of the general purpose phantom obtained using the SSTA image reconstruction method with the MOGCS excitation signals are discussed in Section 3.1, and the conventional STA method with the CGCS and short pulse excitation signals are shown in Fig. 6. The peak-to-peak transmitted voltage was set to a value of 3.2 V to demonstrate the increase in visualisation depth for the MOGCS and CGCS over the short pulse signal for small excitation acoustic power levels. The final reconstructed images (envelopes of the beamformed RF signals corresponding to the image lines) were then normalised to their maximum amplitudes value prior to visualisation.

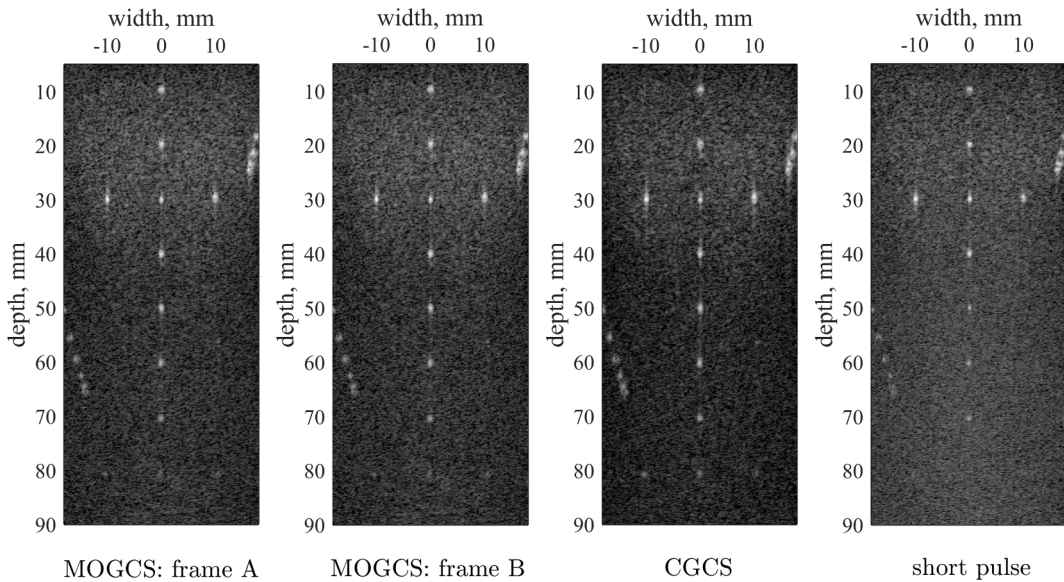


**Fig. 6.** The B-mode images of the general purpose phantom obtained using the SSTA image reconstruction method with the MOGCS excitation signals discussed in the Section 3, and the conventional STA method with the CGCS and short pulse excitation. All images displayed in the log scale over 50 dB dynamic range. The peak-to-peak transmitted voltage was 3.2 V.

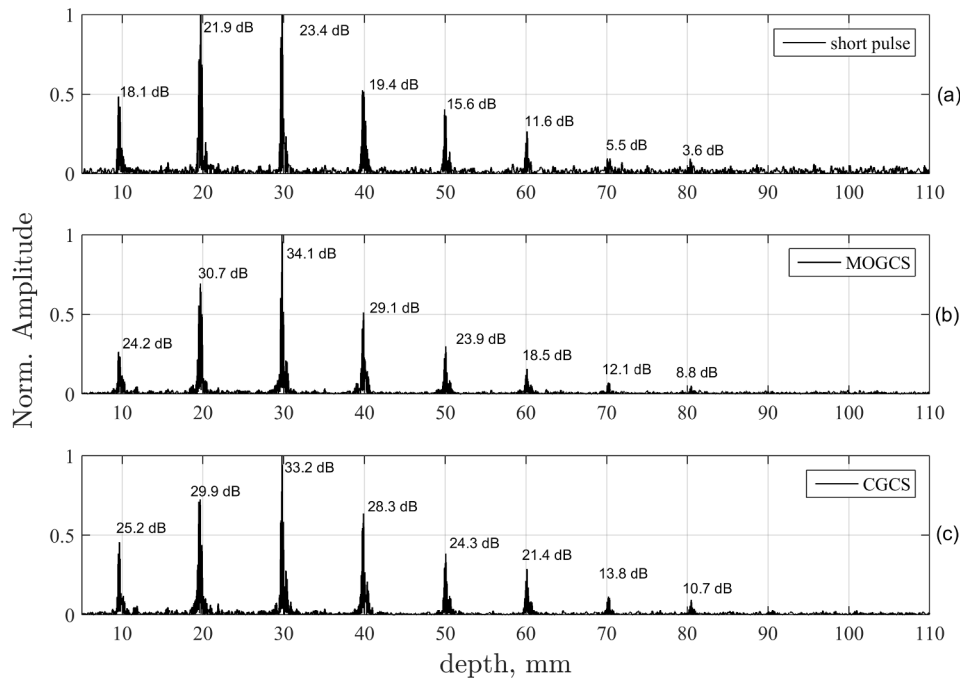


**Fig. 7.** Normalised echo amplitudes along line #64 of the synthesised B-mode images of the general purpose phantom shown in Fig. 6 for the short pulse (a), MOGCS (b) and CGCS (c) transmitted signals. The SNR values determined at different depths are shown.

In Fig. 7, the normalised echoes amplitudes along line #64 of the synthesised B-mode images of the general purpose phantom (see Fig. 6) are shown for different transmitted signals.

Image line #64 coincides with the central column of point scatterers of the general purpose phantom (see Fig. 6), spaced 10 mm along axial direction. In Fig. 8, the SNR determined from the echoes depicted in the Fig. 7 as a function of depth is shown.

As can be seen from Fig. 8 the SNR values for the MOGCS and CGCS transmitted signals did not differ significantly except for the depths above 55 mm where a 2–2.5 dB decrease in the SNR was observed for the MOGCS signal in comparison to the CGCS signal. The corresponding decrease in the SNR value for the short pulse signal varied from about 6 dB to 10.7 dB in the entire considered depth range.

The B-mode images of the cyst phantom obtained using the SSTA image reconstruction method with the MOGCS excitation signals are discussed in the Section 3.1, and the conventional STA method with the CGCS and short pulse excitation signals are shown in Fig. 9. The peak-to-peak transmitted voltage was set to a value of 3.2 V to demonstrate the

increase in visualisation depth for the MOGCS and CGCS over the short pulse signal.

In the case of the MOGCS transmitted signals, two image frames (frames A and B in the Figs. 6 and 9) were synthesised simultaneously.

#### 4.3. In vivo measurements

The B-mode images of the human abdominal aorta and common carotid artery are shown in Figs. 10 and 11. The images were obtained using the SSTA image reconstruction method with the MOGCS excitation signals and the conventional STA method with the CGCS and short pulse excitation signals. The final reconstructed images were then normalised to their maximum amplitude in the image.

To make a comparison of mutual sensitivity of the tested modalities, the received RF signals recorded by a single element of the probe for different transmitted signals are shown in Fig. 12. The recorded echoes were normalised to the maximum value of the CGCS signal to show the range of the amplitude difference.

The peaks of the time-traces depicted in Fig. 12 correspond to the signal reflection from the top surface of the common carotid artery at the depth of 10 mm. The amplitude of echoes recorded using the short pulse were at least five times smaller (-13 dB) than that recorded using CGCS transmission. In the case of the MOGCS excitation signal, the decrease in amplitude was -0.6 dB in comparison to the CGCS signal.

## 5. Discussion

The experimental results presented in this work confirmed the effectiveness of the MOGCS set comprised of two CGCS pairs to be used in ultrasound diagnostic measurements as the transmit signal. It combines the advantages of the CGCS and eliminates its disadvantage, which is the two-fold decrease in the data acquisition and image reconstruction rates. The most important parameters of the recorded RF signals were evaluated and compared for the MOGCS, CGCS and short pulse excitation methods. Specifically, the axial resolution was estimated using the half maximum (measured at the -6 dB level) time duration of the envelopes of the RF signals from the brass plate, shown in Fig. 4. About 9% degradation of axial resolution was observed for the MOGCS in

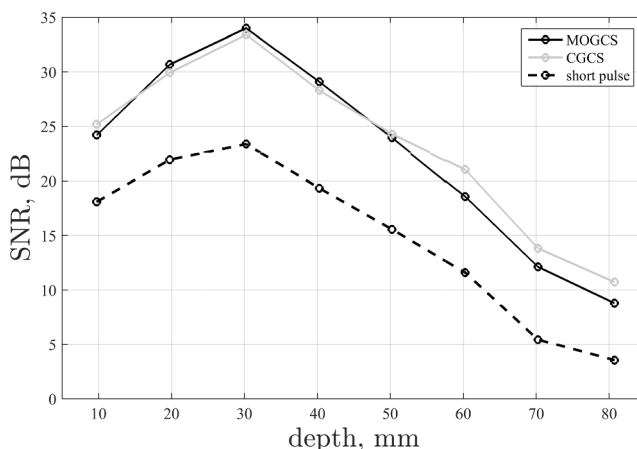


**Fig. 8.** The SNR determined from the echoes along line #64 depicted in Fig. 7 for different transmitted signals.

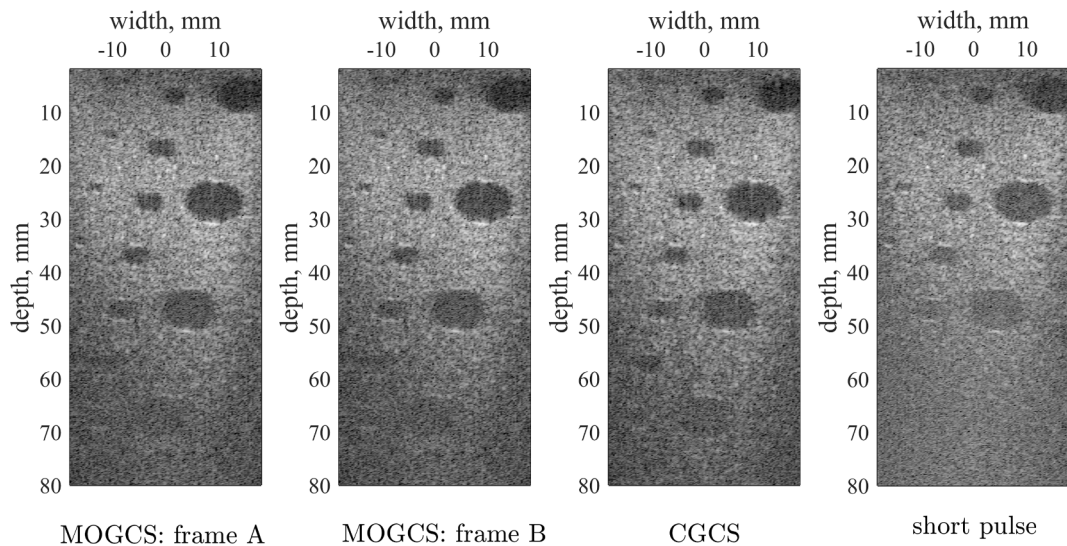


**Fig. 9.** The B-mode images of the cyst phantom obtained using the SSTA image reconstruction method with the MOGCS excitation signals as discussed in the Section 3, and the conventional STA method with the CGCS and short pulse excitation. The cysts with a diameters of 8 mm, 4 mm and 2 mm are visualised. All images displayed in the log scale over 50 dB dynamic range. The peak-to-peak transmitted voltage was 3.2 V.

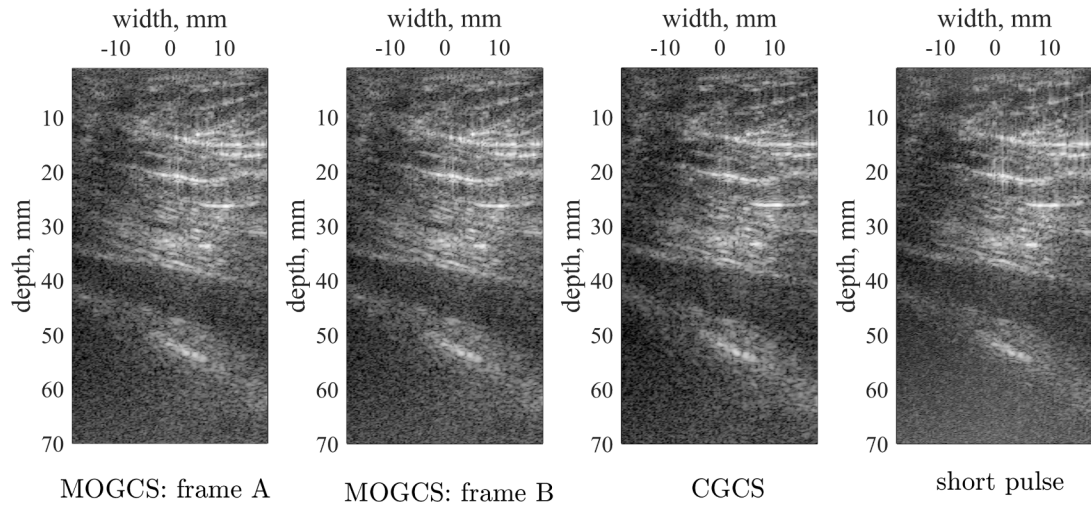


**Fig. 10.** B-mode images of the experimental data acquired in vivo from the human abdominal aorta obtained using the SSTA image reconstruction method with the MOGCS excitation signals as discussed in Section 3, and the conventional STA method with the CGCS and short pulse excitation. All images are displayed in the log scale over a 60 dB dynamic range. The peak-to-peak transmitted voltage was 20 V.

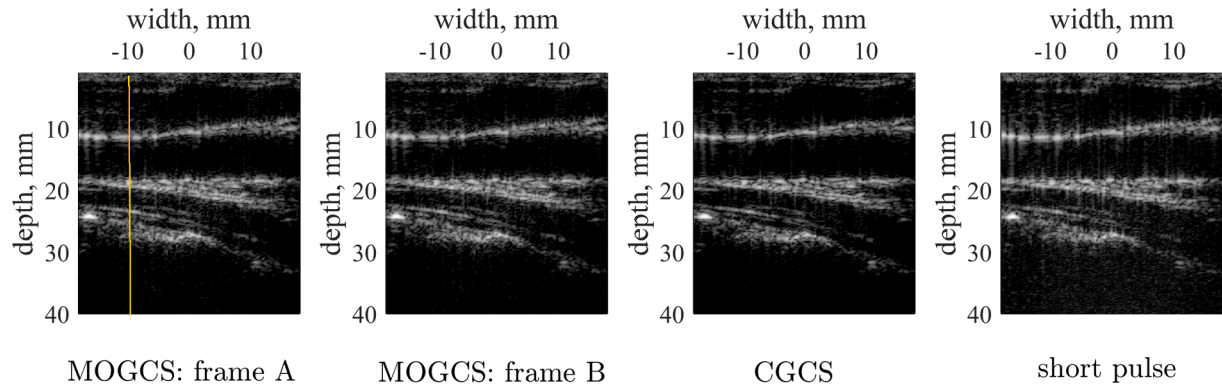


**Fig. 11.** The B-mode images of the experimental data acquired in vivo from the human common carotid artery obtained using the SSTA image reconstruction method with the MOGCS excitation signals as discussed in Section 3, and the conventional STA method with the CGCS and short pulse excitation. All images are displayed in the log scale over a 40 dB dynamic range. The peak-to-peak transmitted voltage was 20 V. The vertical line in the leftmost panel indicates the position of the RF echoes depicted in Fig. 12.

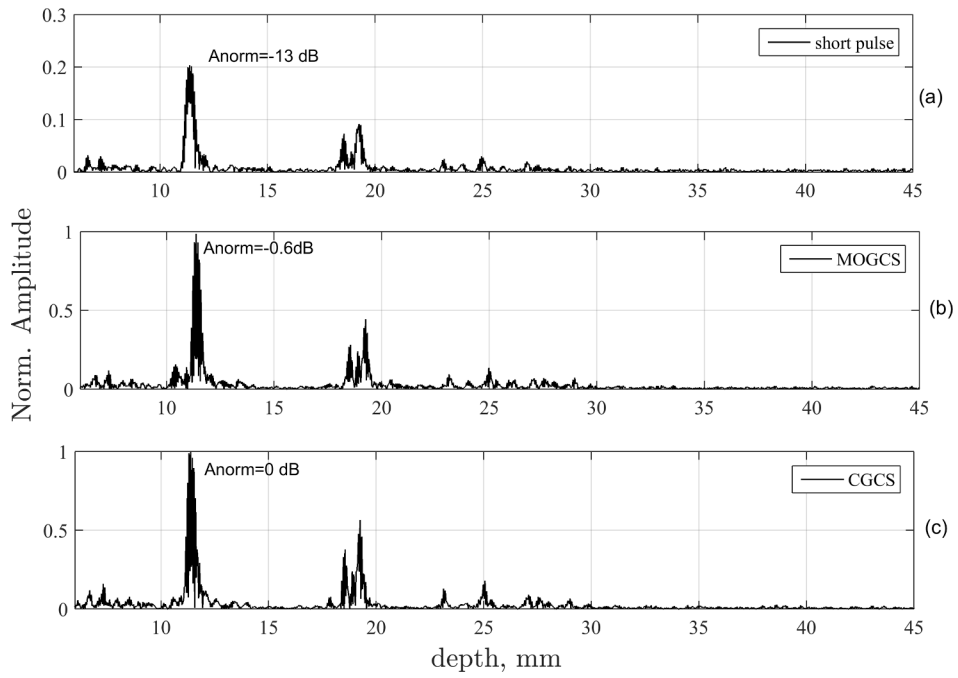


**Fig. 12.** Magnitude of the processed RF echoes from the human common carotid artery shown in Fig. 11 for the short pulse (a), MOGCS (b) and CGCS (c) transmitted signals. The echoes were recorded with element #31 (marked with a vertical line in the leftmost panel in Fig. 11) during transmission #16 in the STA data acquisition scheme (see discussion in Section 3.1).

comparison to the conventional CGCS signal. The spatial duration of the compressed signals increased from 0.46 mm for the CGCS to 0.51 mm for the MOGCS signal. In the case of the short pulse excitation, 17% and 8.3% degradation of axial resolution was observed in comparison to the CGCS and MOGCS signals, respectively. The spatial duration of the short pulse was 0.55 mm.

The side lobe level (SLL) was estimated from the envelopes of the RF signals reflected from the brass plate immersed in degassed water. As can be seen from Fig. 4, the SLL of the MOGCS compressed signal was about  $-20.6$  dB. The corresponding values for the CGCS and the short pulse were about  $-22.1$  dB and  $-20.1$  dB, respectively. These results confirm the efficiency of side-lobe cancelation due to matched filtering and compression of the coded transmitted signals.

The SNR values for the MOGCS, CGCS and short pulse transmitted signals were compared using RF echoes recorded by a single element of the probe from a general purpose phantom. Very similar SNR values were obtained for the CGCS and MOGCS signals at the depth of 10 mm, whereas at the 20 mm depth the SNR of the CGCS signal was 1.3 dB higher than the SNR of the MOGCS signal. On the other hand, at a depth of 30 mm, the MOGCS signal had 1.9 dB better SNR than the CGCS. In the case of the short pulse signal, 5.2 dB and 4.6 dB decreases in the SNR in comparison with the MOGCS signal were observed, which corresponded to 24% and 35% degradation of the SNR. Also, the SNR values at different depths were determined from the echoes (see Fig. 7) along line #64 of the synthesised B-mode images of the general purpose phantom. Again, it can be seen from Fig. 8 that the SNR values obtained using the MOGCS and CGCS transmit signals did not differ much. Maximum degradation of the SNR corresponding to the MOGCS echoes was observed at depths above 55 mm and was about 2.5 dB. Moreover, the coded transmission using CGCS and MOGCS yielded an increase in the SNR from 6 dB to 10.7 dB over the short pulse signal for the entire range of depths considered. A slight decrease in the SNR value at a depth of 10 mm can be observed in Fig. 8 for all three modalities. This deterioration of the SNR as well as the decrease in the signal amplitude, shown in Fig. 7, can be explained by the fact that the coherent summation of the RF signals from different transmit and receive sub-apertures in the STA image reconstruction method becomes less

effective and burdened with large errors in the vicinity of the transducer face [21].

Finally, the proposed SSTA method was tested using experimental data obtained from the general purpose and cyst phantoms, and the data acquired *in vivo* from human abdominal aorta and common carotid artery measurements. Specifically, the results obtained for the MOGCS signal are shown in the Fig. 6 and Fig. 9 through Fig. 11 (frames A and B). The images were reconstructed simultaneously as discussed in Section 3.1, thus enabling the synthesis of two image frames from acoustic echoes obtained during a single data acquisition cycle. For comparison, the B-mode images obtained using the conventional STA with CGSS and short pulse transmitted signals are also shown. It can be seen (by visual assessment) that the proposed SSTA method with the MOGCS signal allows for obtaining two frames of the comparable quality to those obtained using the conventional CGCS signal. This allows the frame rate to be increased twice by using the MOGCS set in comparison to the conventional CGCS, maintaining better visualisation depth in comparison to the short pulse transmit signal at the same time. Also, it can be seen from Fig. 9 that both the MOGCS and CGCS interrogating signals better perceived the visualisation depth of cysts located at depths greater than 50 mm. The resolution of the B-mode images was similar for different excitation signals. In a standard clinical application, a rather higher frequency (over 7 MHz) would be used to acquire carotid scans, while the abdominal aorta would be examined using a convex transducer. However, the purpose of our *in vivo* experiment was only to show that the introduction of the MOGCS imaging system does not deteriorate the quality of the imaging with naturally better sensitivity and depth of penetration.

## 6. Conclusions

In this work, we conducted a comparative analysis using experimentally obtained acoustic data to confirm that, by using two CGCS pairs constituting the MOGCS set, the data acquisition and frame rates can be increased two-fold in comparison with conventional CGCS. Specifically, the SSTA method proposed in this paper, which uses the MOGCS transmit signal, has shown the possibility of simultaneous

reconstruction of two image frames from a single data acquisition cycle without a noticeable decrease in image quality. Moreover, despite simultaneous transmission of two different interrogating signals, efficient extraction of the echoes corresponding to different codes of the MOGCS set was demonstrated experimentally. For this purpose, the SNR, the SLL and axial resolution of the compressed echoes resulting from simultaneous transmission of two sets of 16-bit long CGCS signals comprising the MOGCS set, successive transmission of the conventional CGCS pair and the short pulse transmission were evaluated and compared. The results confirmed that simultaneous transmission of the MOGCS and extraction of the combined RF echoes on the receiver side does not worsen the parameters of the signals in comparison to conventional CGCS. At the same time, transmission of the MOGCS sets allows for maintaining the axial resolution and data acquisition speed, as in the case of the short pulse transmission. Moreover, using the CGCS and MOGCS transmitted signals combined with compression of the received echoes allowed the SNR to be increased without increasing the transmitted amplitude [29]. Hence, the high peak power of the interrogating signal is no longer required. The gain in SNR and visualisation depth increase in comparison to the short pulse result from the compression of the CGCS and MOGCS echoes. This is the advantage of the CGCS and MOGCS over the short pulse interrogating signal, i.e. that more acoustic energy can be transmitted without increasing the peak transmitted power.

These results experimentally demonstrate the advantage of the MOGCS for use in modern ultrasound diagnostics compared to the conventional short pulse and CGCS excitation signals.

### Declaration of Competing Interest

The authors declare that they have no known competing financial interests or personal relationships that could have appeared to influence the work reported in this paper.

### References

- [1] S. Chen, K.J. Parker, Enhanced axial and lateral resolution using stabilized pulses, *J. Med. Imaging* 4 (2017), 027001.
- [2] F.T. D'Astous, F.S. Foster, Frequency dependence of ultrasound attenuation and backscatter in breast tissue, *Ultrasound Med. Biol.* 12 (1986) 795-808.
- [3] A. Nowicki, W. Secomski, J. Litniewski, I. Trots, On the application of signal compression using Golay's codes sequences in ultrasound diagnostic, *Arch. Acoust.* 28 (2003) 313-324.
- [4] I. Trots, Y. Tasinkeyvych, A. Nowicki, M. Lewandowski, Golay coded sequences in synthetic aperture imaging systems, *Arch. Acoust.* 36 (2011) 913-926.
- [5] M. O'Donnell, Coded excitation system for improving the penetration of real array imaging systems, *IEEE Trans. Ultrason. Ferroelectr. Freq. Contr.* 39 (1992) 341-351.
- [6] B. Haider, Peter A. Lewin, Kai E. Thommenius, Pulse elongation and deconvolution filtering for medical ultrasonic imaging, *IEEE Trans. Ultrason. Ferroelectr. Freq. Contr.* 45 (1998) 98-113.
- [7] M. Pollakowski, H. Ermert, Chirp signal matching and signal power optimization in pulse-echo mode ultrasonic nondestructive testing, *IEEE Trans. Ultrason. Ferroelectr. Freq. Contr.* 41 (5) (1994) 655-659.
- [8] T. X. Misaridis, Kim Gammelmark, C. H. Jorgensen, N. Lindberg, A. H. Thomsen, M. H. Pedersen, J. A. Jensen, Potential of coded excitation in medical ultrasound imaging, *Ultrasonics* 38 (2000) 183-189.
- [9] S. Zhou, X.C. Wang, J. Yang, J.J. Ji, Y.Q. Wang, Barker-coded excitation in ophthalmological ultrasound imaging, *Int. J. Clin. Exp. Med.* 7 (2014) 2413-2424.
- [10] H. K. Zhang, K. Kondo, M. Yamakawa, T. Shiina, Coded excitation using periodic and unipolar M-sequences for photoacoustic imaging and flow measurement, *Opt. Express* 24 (2016) 17-29.
- [11] M. J. E. Golay, Complementary series, *IRE Tran. Inf. Theory* 7 (1961) 82-87.
- [12] I. Trots, A. Nowicki, W. Secomski, J. Litniewski, Golay sequences - side-lobe canceling codes for ultrasonography, *Arch. Acoust.* 29 (2004) 87-97.
- [13] I. Trots, Y. Tasinkeyvych, A. Nowicki, Orthogonal Golay codes with local beam pattern correction in ultrasonic imaging, *IEEE Signal Process. Lett.* 22 (2015) 1681-1684.
- [14] X. Huang, Complementary properties of Hadamard matrices, in Proc. of 2006 International Conference on Communications, Circuits Syst. 1 (2006) 588-592.
- [15] M.-H. Bae, W.-Y. Lee, M.-K. Jeong, S.-J. Kwon, Orthogonal Golay code based ultrasonic imaging without reducing frame rate, *Proc. IEEE Ultrason. Symp.* (2002) 1705-1708.
- [16] B.-H. Kim, T.-K. Song, Multiple transmit focusing using modified orthogonal Golay codes for small scale systems, *IEEE Int. Ultrason. Symp.* (2003) 1574-1577.
- [17] H. Peng, X. Han, J. Lu, Study on application of complementary Golay code into high frame rate ultrasonic imaging system, *Ultrasonics* 44 (2006) e93-e96.
- [18] F. Zhao, J. Luo, Diverging wave compounding with spatio-temporal encoding using orthogonal Golay pairs for high frame rate imaging, *Ultrasonics* 89 (2018) 155-165.
- [19] C.R. Cooley, B.S. Robinson, Synthetic focus imaging using partial datasets, *Proc. IEEE Ultrason. Symp.* (1994) 1539-1542.
- [20] G. R. Lockwood and F. S. Foster, Design of sparse array imaging systems, in Proc. IEEE Ultrason. Symp. (1995) 1237-1243.
- [21] Y. Tasinkeyvych, Z. Klimonda, M. Lewandowski, A. Nowicki, P.A. Lewin, Modified multi-element synthetic transmit aperture method for ultrasound imaging: A tissue phantom study, *Ultrasonics* 53 (2013) 570-579.
- [22] I. Trots, Y. Tasinkeyvych, A. Nowicki, M. Lewandowski, Coded transmission in synthetic transmit aperture ultrasound imaging method, *World Acad. Sci. Eng. Technol.* 63 (2012) 331-336.
- [23] R.Y. Chiao, L.J. Thomas, Synthetic transmit aperture imaging using orthogonal Golay coded excitation, *Proc. IEEE Ultrason. Symp.* (2000) 1677-1680.
- [24] I. Trots, Mutually orthogonal Golay complementary sequences in synthetic aperture imaging systems, *Arch. Acoust.* 40 (2015) 283-289.
- [25] <http://www.fantom.dk/525.htm>.
- [26] <http://www.fantom.dk/571.htm>.
- [27] C. C. Tseng and C. L. Liu, Complementary sets of sequences, *IEEE Trans. Info. Theory* 18 (1972) 644-652.
- [28] T. Misaridis, Ultrasound imaging using coded signals, Center for fast ultrasound imaging technical university of Denmark, PhD Thesis, 194 pages, (2001).
- [29] A. Nowicki, W. Secomski, J. Litniewski, I. Trots, P.A. Lewin, On the application of signal compression using Golay's codes sequences in ultrasound diagnostic, *Arch. Acoust.* 28 (2003) 313-324.